Applied Physics Letters ARTICLE scitation.org/journal/apl

Carbon nanotube thermoelectric devices by direct printing: Toward wearable energy converters

Cite as: Appl. Phys. Lett. **118**, 173901 (2021); doi: 10.1063/5.0042349
Submitted: 29 December 2020 · Accepted: 6 March 2021 ·
Published Online: 27 April 2021

Hye Ryoung Lee,[1,2,a)] Naoki Furukawa,[1,3] Antonio J. Ricco,[1] Eric Pop,[1] Yi Cui,[2,4,a)] and Yoshio Nishi[1]

AFFILIATIONS

[1]Department of Electrical Engineering, Stanford University, Stanford, California 94305, USA
[2]Stanford Institute for Materials and Energy Sciences, SLAC National Accelerator Laboratory, Menlo Park, California 94025, USA
[3]Daihen Corporation, Osaka 5328512, Japan
[4]Department of Materials Science and Engineering, Stanford University, Stanford, California 94305, USA

[a)]**Authors to whom correspondence should be addressed:** hyeryoung.lee@stanford.edu; and yicui@stanford.edu

ABSTRACT

Thermoelectric devices convert thermal energy to electrical energy and are particularly well-suited for energy harvesting from waste heat. Even as the number of electronic devices used in daily life proliferates, technical advances diminish the average power such devices require to perform a given function. Localized thermal gradients that abound in our living environments, despite having modest energy densities, are therefore becoming increasingly viable and attractive to power such devices. With this motivation, we report the design, fabrication, and characterization of single-wall carbon nanotube thermoelectric devices (CNT-TDs) on flexible polyimide substrates as a basis for wearable energy converters. Our aqueous-solution-based film fabrication process could enable readily scalable, low-cost TDs; here, we demonstrate CNT-hydroxypropyl cellulose (HPC) composite thermoelectric films by aerosol jet printing. The electrical conductivity of the composite films is controlled through the number of CNT/HPC layers printed in combination with control of the annealing conditions. The HPC initially disperses the CNTs in deionized water, the greenest of solvents, and is subsequently partially eliminated from the film by annealing, with concomitant morphological changes that we characterized by TEM. HPC removal is key to obtaining good electrical conductivity (0.94 to 1.10×10^5 S/m) and Seebeck coefficients (36 to 43 μV/K). We also report a power factor of 208 μW m^{-1} K^{-2} for a CNT-TD composed of 15 layers of CNT/HPC, promising performance for CNT-based flexible TDs that are deposited from aqueous solution, stable in air, and require no additional doping or sorting processes.

Localized energy use in modern society is proliferating as a wide variety of portable and wearable electronic devices, many of them nodes on the internet of things (IoT), become part of daily life. Increasing total energy demand presents a significant challenge, however: non-renewable energy sources have long-term limitations due to finite supply and environmental impact; sustainable, renewable energy sources, while gaining both societal support and share of total energy usage, are not without cost to implement. Accordingly, the current timeline for phase-out of fossil energy is perilously long.

Reducing total energy demand could help address this challenge: according to a March 2020 report, about 67.5% of energy generation was wasted in 2019, primarily as heat.[1] Utilizing waste heat for local energy harvesting could speed the process of converting an ever-larger percentage of energy generation to non-fossil, sustainable energy sources.

Using existing thermal gradients, including those associated with waste heat, as a source of electrical energy is a potentially ubiquitous contributor to improvements in overall energy utilization efficiency. The diversity of sources includes motors of all types, high-intensity lighting (including LEDs), hot-water pipes, vehicle engines or exhaust, industrial and manufacturing equipment, power plants, computer servers, heated roads, and even human bodies. The desire to tap these largely unutilized sources of electricity is now focusing increasing attention on thermoelectric device research.

Three significant obstacles must be overcome for widespread implementation of local thermoelectric power conversion: low conversion efficiencies, use of toxic and otherwise challenging materials, and the (anticipated) cost of volume manufacturing. Most of today's thermoelectric devices are made of inorganic semiconductors and their alloys, including Bi_2Te_3, PbTe, and Sb_2Te_3,[2,3] materials that are toxic, expensive, brittle, and of limited natural abundance. Together, these issues are driving researchers to explore a variety of new, "greener" thermoelectric materials that

may yield improved efficiency,[4,5] as well as compatibility with economically viable manufacturing scenarios.

Carbon-based materials are particularly attractive as an alternative for thermoelectrics due to their nontoxicity, abundance, solution processability, and potential for high specific energy density (due to low mass density).[2] Significant research has focused on lightweight, flexible thermoelectric devices based on conducting organic polymers; some have demonstrated promising performance.[3,6–11] They are generally susceptible, however, to thermal and/or oxidative degradation, and some are potentially challenging to manufacture at low cost and high volume.[2]

Among the carbon-based materials potentially suited for thermoelectric converters, carbon nanotubes (CNTs) are promising for their high electrical conductivity, mechanical robustness and flexibility, chemical and thermal stability, and solution-processability: they can be functionalized to form stable dispersions for printable inks,[4] or dispersed in solvents, with addition of a solubilizing component where necessary, to enable thin-film formation by printing. CNTs were first discovered in 1991, followed by isolation of single-wall CNTs in 1993.[12,13] Since then, researchers have tuned the electrical and thermal conductivities of CNTs by sorting, doping, and mixing them with polymer materials.[14–18] In addition, semiconducting single-wall CNTs within such composites are expected to have particularly large Seebeck coefficients due to one-dimensional confinement, which imposes a large asymmetry in the density of states near the Fermi level.[19,20]

The figure of merit for thermoelectric energy harvesters is $ZT = S^2\sigma T/\kappa$, where S is the Seebeck coefficient, σ is the electrical conductivity, T is the absolute temperature, and κ is the thermal conductivity. CNTs, in particular, have been reported to have good thermoelectric power factors ($P = S^2\sigma$, in units of $\mathrm{Wm^{-1}K^{-2}}$), when sorted and doped to ensure adequate conductivity.[21–24] While doping with other materials, provided they are not hazardous or costly, is not necessarily a significant impediment to manufacturability, the process would be simpler and potentially more robust if this were not necessary; the need to sort the CNTs is unquestionably an added cost to be avoided if possible.

Here, we demonstrate flexible CNT thermoelectric devices fabricated by all-aqueous-solution processing and directly printed CNT inks on flexible polyimide (PI) substrates. Such water-based processing is particularly promising for green, large-scale, low-cost, flexible device fabrication due to not only its compatibility with printing technology but also the absence of vacuum processing.

CNTs were made by an enhanced direct-injection pyrolytic synthesis (eDIPS) method at Meijo Nano Carbon. This method offers good diameter control of CNTs through its two-step growth conditions and use of relatively fine, homogeneous nanoparticles as catalysts.[25] Figure S1 shows scanning electron microscope (SEM) images of the original, as-received shapes of "large" bundles of CNTs and an enlarged image of the bundled CNTs. These materials are more than 99% pure carbon, the majority are single-wall CNTs, and they were used without further sorting or doping.

Homogeneous dispersion of CNTs is essential to make printable inks that provide consistent results. Various organic solvents have been used to disperse CNTs with promising results, but aqueous solvents are preferable due to lower cost, lack of toxicity, and ease of manufacturing without a closed, vapor-emission-controlled environment. In this work, CNT bundles were dispersed in deionized (DI) water; hydroxypropyl cellulose (HPC; Sigma-Aldrich) was added to ensure uniform dispersion. A cellulose derivative with good solubility in a wide variety of solvents including water,[26] HPC, is added to many commercial products including cosmetics, foods, edible coatings and films,[27,28] pharmaceuticals, and "artificial tears" formulations. This "edible polymer" lacks toxicity or other adverse human effects, and it has also been shown over the past decade to be an effective dispersant for nanomaterials including CNTs.[29,30]

The CNT/HPC ink formulation was optimized by controlling concentrations, HPC to CNT ratio, sonication power and time (to make a uniform dispersion), and centrifuge conditions (to remove agglomerates from the otherwise-uniform dispersion). Optimal results were ultimately obtained when HPC and CNTs were mixed in a 2:1 mass ratio and dispersed in DI water at a combined concentration of 0.8% by weight using a probe sonicator at 100 W for 3 h, resulting in a stable ink. The ink was then centrifuged at 7500 rpm for 30 min to remove large agglomerates of CNT/HPC. Figures 1(a) and 1(b) show transmission electron microscope (TEM) images of the CNT/HPC ink, revealing that the CNTs are not all individually dispersed but exist as much finer CNT bundles in the ink compared to the original large bundles. The average diameter of CNTs measured from TEM images is 1.73 ± 0.09 nm.

To make devices, an aerosol-jet printer (AJP; AJ 300, Optomec) was first used to pattern CNT/HPC inks. AJP directly patterns devices without masks, allows control of film thickness via the number of layers printed, and has less stringent requirements for ink properties than many other printing methods: viscosity can be in the 1–1000 cP range using the AJP's pneumatic atomizer. Thick films are readily made with minimal loss of materials[3] and conformal patterning of films on 3D objects is possible via dynamic print-head angle control.[31–33] The setup of the AJP pneumatic atomizer, Fig. 2, shows aerosol formation from the inks and the aerosol flow path to the deposition head. Prior to printing, substrates were oxygen-plasma cleaned (3 min at 35 W, PE-50 system). CNT inks were then printed on both 127 μm-thick PI films and on SiO_2/Si substrates.

After AJP printing, hot-plate annealing was used to eliminate a controlled fraction of the HPC in order to improve the electrical conductivity of CNT films without conferring excessive thermal conductivity. Annealing temperatures of 350 °C or above in air, which result in significant degradation (and elimination) of HPC together with formation of "char,"[34,35] yielded promising electrical conductivity values, while maintaining good Seebeck coefficients. Figure 3 shows thermogravimetric analysis (TGA) results in air for the HPC polymer alone,

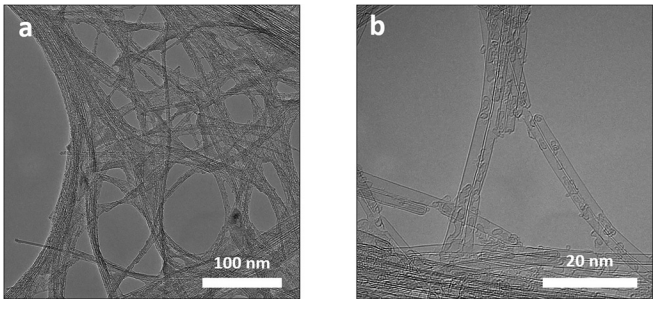

FIG. 1. TEM images: (a) CNT/HPC ink (b) enlargement of part of image (a).

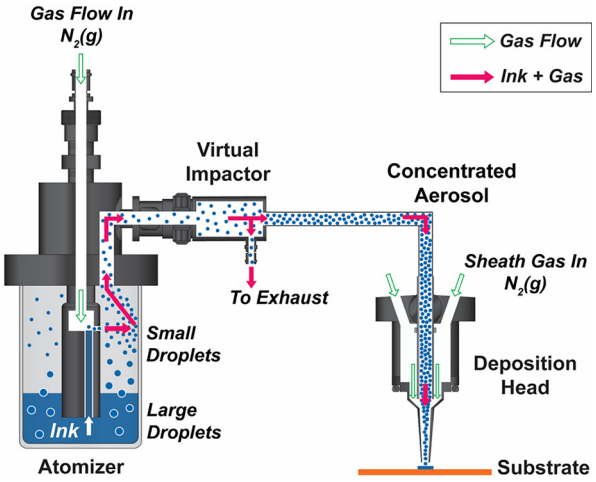

FIG. 2. Schematic diagram of aerosol jet printing. The pneumatic atomizer shears an ink to small droplets through a high-velocity gas stream. A virtual impactor concentrates the aerosol stream by eliminating excess atomization gas from the system. The output of the virtual impactor is connected to the print head.

which guided the choice of an appropriate annealing temperature. Ultimately, annealing was conducted at 350 °C in air for various time lengths, removing the majority of HPC.

Figure 4(a) shows examples of CNT/HPC aerosol droplets made on a SiO_2 (on Si wafer) substrate using the AJ 300. Spherical aerosol particles make circular droplets of varying sizes on SiO_2 and PI substrates. As shown in Fig. 4(b), the average CNT/HPC aerosol droplet size in this case was 4.4 μm with a range of 1.4–13.8 μm measured from 57 droplets in three different areas. Figure 4(c) shows that the printed CNTs within the film are quite uniform, lacking any significant aggregation, and randomly oriented. Figure 4(d) shows the CNT/HPC film thickness as a function of annealing time. After 30–60 min of annealing, film thicknesses were reduced dramatically due to dehydration and HPC decomposition/elimination.

To understand the impact of annealing on the CNT/HPC network, we performed TEM experiments, imaging the CNT/HPC network morphologies before and after annealing. CNT/HPC in DI

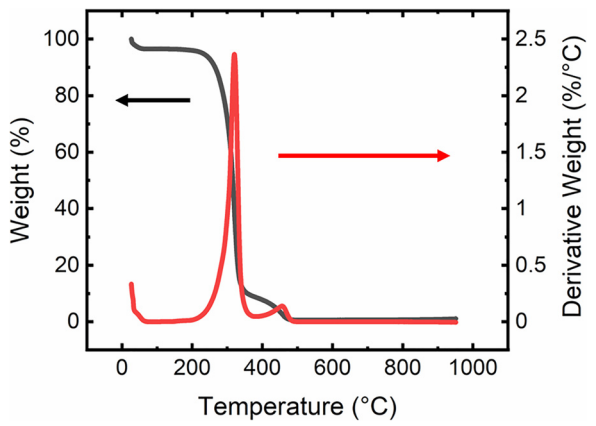

FIG. 3. Thermogravimetric Analysis (TGA) results of the HPC polymer.

water was dropcast on a TEM heating chip (DENSsolutions; images of the heating chip and sample loading configurations are shown in Fig. S4). After drying the ink at room temperature, the heating chip with CNT/HPC samples was inserted into the TEM column and imaged. Figure 4(e) shows that HPC covers most CNT areas. After initial imaging, the sample was removed from the TEM column and annealed in air at 350 °C, our usual process, for 60 min, then re-inserted in the TEM column and imaged. Figure 4(f) shows a CNT/HPC image after the annealing at the same area imaged before annealing. The changes from Figs. 4(e) and 4(f) are a consequence of the removal of much of the HPC polymer, presumably via oxygen-assisted thermal decomposition.

In the process of device fabrication, after the CNT/HPC film was annealed, Ag contacts were inkjet printed, a straightforward process that uses well-developed conditions and inks to make very conductive Ag layers. Electrodes were printed from Ag ink (JS-A102A, Novacentrix) with a Model 2800 printer (FUJIFILM Dimatix) at the two edges of the CNT/HPC films [Fig. S2(a)]. The entire structure was then annealed on a hot plate in air at 120 °C for 30 min to cure the Ag ink and ensure good contact to the CNT film.

Optical images of the printed CNT thermoelectric devices and arrays are shown in Fig. 5(a). (Supplementary material Fig. S2 also displays the inkjet-printed Ag area, the overlapped Ag and CNT/HPC contact area, and the aerosol-jet-printed CNT/HPC area.) Electrical measurements reveal good ohmic contacts, i.e., no rectifying behavior, as shown in Fig. S3. To understand whether there is any difference when the CNT/HPC region is beneath the Ag electrodes [the area in Fig. S2(c)] rather than on top of them, Ag contacts were printed both before and after CNT/HPC printing. Both cases showed good ohmic contacts without significant differences due to the printing sequence.

Figures 5(b)–5(d) display the measured CNT-TD thermoelectric performance parameters. Figure 5(b) reveals a general improvement of the Seebeck coefficient with increasing annealing time. Five-layer printed CNT/HPC films showed a 19% increase in Seebeck coefficient relative to their initial values in the first 30 min of annealing. Ten- and 15-layer films showed 23% and 27% improvements, respectively, after 30 min of annealing. After 90 min of annealing, the five-, ten-, and 15-layer films revealed 26%, 30%, and 44% respective enhancements in their Seebeck coefficients. Figures 5(c) and 5(d) show that the power factor and electrical conductivity also generally improve as a function of annealing time.

After exploring the range of ink formulations and printing conditions described above, a maximum power factor of 208 μW m^{-1} K^{-2} was ultimately obtained from a 15-layer CNT-TD (represented by the "15 L" curves of Fig. 5). The power factor, $S^2\sigma$, where S is the Seebeck coefficient and σ the electrical conductivity, is calculated from our S and σ measurements at room temperature. These power factors are as good or better than those reported for doped-CNT thermoelectric devices made using CNTs from the same commercial source.[36,37] Our improvement mainly comes from the increased electrical conductivity after annealing the CNT-TDs. CNTs are known to be doped by oxygen treatment, e.g., water-vapor or KOH processing is often used to provide oxygen doping of CNTs.[37] Our device preparation process did not include any deliberate oxygen-doping step, but such doping could have occurred during the air-annealing process as water was removed and the HPC was decomposed or degraded in order to improve the electrical conductivity of the film.

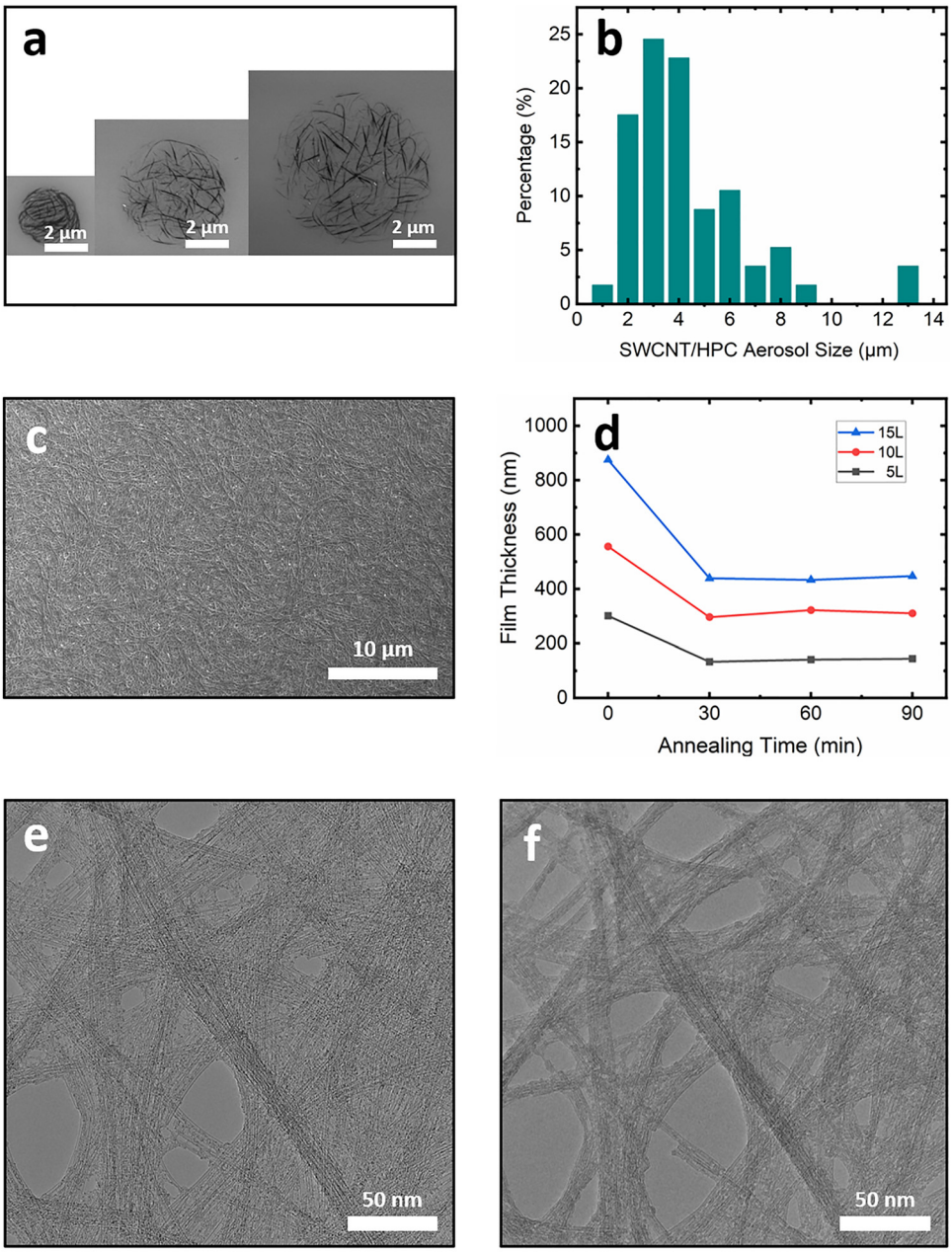

FIG. 4. (a) SEM images of individual aerosol droplets of CNT/HPC ink with three typical sizes found on the SiO_2 substrate, (b) CNT/HPC aerosol size distribution, and (c) an SEM top view image of 15-layer (15 L) film of printed CNT/HPC, which does not show individual droplets and is uniform in appearance. (d) Film thickness of printed CNT/HPC as a function of annealing time, for samples with various layers. Annealing temperature was 350 °C in air for all samples. TEM images of CNT/HPC (e) before and (f) after 350 °C in air heating for 60 min.

We believe the improved CNT-film electrical conductivity is in part a result of the finer CNT bundles in our films (i.e., fewer tubes per bundle) that result from prolonged centrifugation. In addition, the aerosol formation process is likely to reduce the amount of agglomeration compared to CNT inks prepared by filtration, which can result in greater agglomeration and thicker CNT bundles.

We used CNTs as-received without additional sorting or doping processes, which means, statistically, that a certain fraction (up to approximately two-thirds) is semiconducting. It has been shown, both experimentally and theoretically,[2,21] that semiconducting CNTs (s-CNTs) have higher Seebeck coefficients due to the sharp increase in the density of states near the Fermi energy level than metallic CNTs

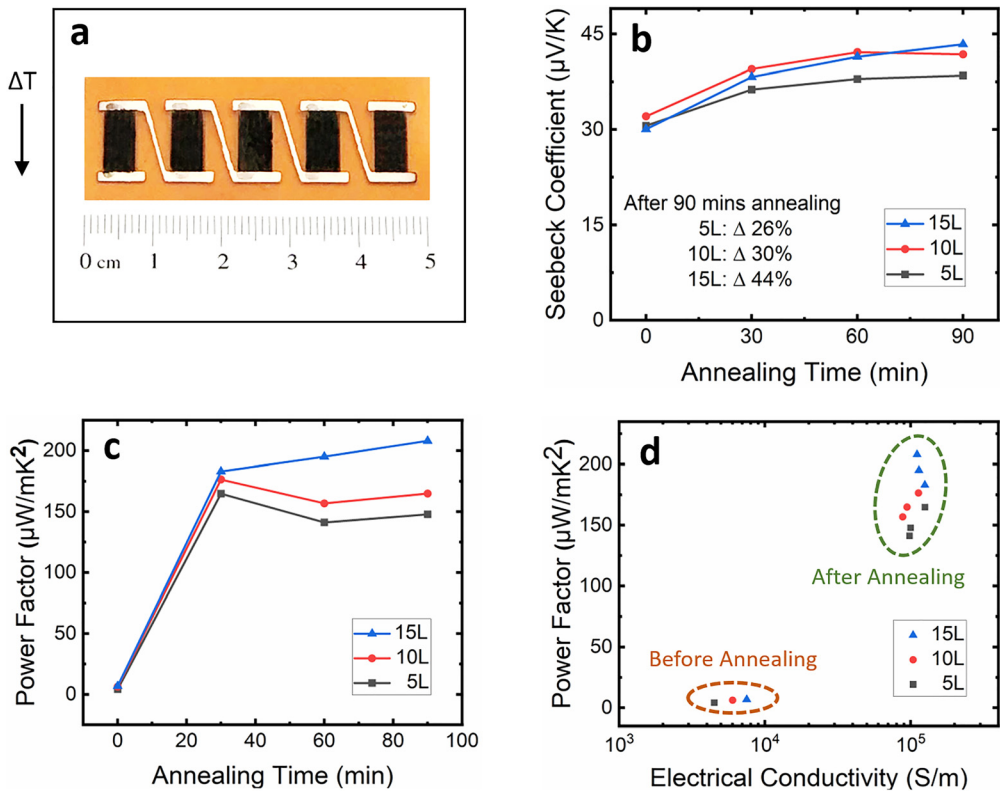

FIG. 5. (a) An optical image of an array of devices. The vertical arrow shows the temperature gradient applied during testing. (b) Measured Seebeck coefficient S and (c) power factor $S^2\sigma$ dependence on annealing time for a single device. (d) Measured power factor as a function of electrical conductivity for a single device. Annealing temperature was 350 °C in air for all samples. 5 L, 10 L, and 15 L are the number of printed CNT/HPC film layers.

(m-CNTs). On the other hand, the electrical conductivity of s-CNT films is lower than those made from m-CNTs, which are a component of the unsorted CNTs. Consequently, systematic optimization will be necessary to uncover the ratio of s-CNTs to m-CNTs that provides optimal thermoelectric performance; the ideal ratio may differ according to the specific material systems, geometries of films and devices, and processing methods used.

The characteristics of CNTs vary considerably depending on the growth method and post processing; therefore, it is not straightforward to compare thermoelectric performance from multiple s-CNT to m-CNT ratios if the CNTs were made with different growth conditions and the CNT-based thermoelectric devices were prepared using diverse fabrication methods. A recent study compared the effect of s-CNTs on thermoelectric performance from unsorted, s- and m-CNTs, which were obtained from similar CNT growth conditions and fabrication methods, revealing that 98% s-CNTs improved the thermoelectric performance compared to s-CNTs with low purity (2%, 33%, 67%, and 80%), m-CNTs or unsorted CNTs.[38] While these results show that the s-CNTs with high purity provide better thermoelectric device performance, they also reveal that the unsorted CNTs have promising performance. Considering the additional processing time, materials loss during sorting, and undesirable defects in sorted CNTs, unsorted CNTs are a good option when the performance difference is insignificant; the performance differences will generally need to be measured and their impact evaluated for each CNT-based thermoelectric device.

Doping CNTs has been actively researched as a means to improve electrical conductivity or to change the majority carrier from holes to electrons to make n-type CNTs. Promising thermoelectric performance has been reported using doped CNTs, but the long-term stability of such chemically doped devices will need to be improved to support practical thermoelectric device applications through designing dopant chemistry and/or the addition of passivation layers.[39]

Although individual CNTs have high thermal conductivity, CNT networks and films show much lower thermal conductivity because of high thermal resistance at CNT–CNT contacts.[40–42] Moreover, our CNT/HPC networks include some (partially degraded) HPC, which has low thermal conductivity but adequate electrical conductivity due to charring. We expect control of CNT/HPC networks to be essential for the improvement of thermoelectric performance; for example, it has been reported that network morphology is a more important factor than chirality in determining the thermal conductivity of CNT networks.[42] Whether the inclusion of metallic CNTs acting as conductive "bridges" between s-CNTs impacts performance and whether improving the conductivity of s-CNTs by doping might (further) improve performance will need to be investigated by comparing results using sorted s-CNTs with defined ratios of s- to m-CNTs and by characterizing the results of additional doping.

Thermoelectric devices convert wasted heat to useful electrical energy. To be widely used to reduce net energy consumption in modern society, it is important to find high-performance thermoelectric materials, low-cost fabrication methods, and applications where the characteristics of these devices provide a significant advantage due to ease of use, cost savings, or both.

We explored the use of CNTs as thermoelectric materials due to their high electrical conductivity, mechanical stability, chemical stability, flexibility, and solution processability when combined with an appropriate dispersion agent, HPC. At the same time, we defined and optimized a direct printing process for CNT-TDs with the goal of enabling future low-cost, high-volume device manufacturing: all materials were solution-processed and no masks were required for patterning, which are important for high-performance, cost-effective, and scalable manufacturing of CNT-TDs.

These flexible, lightweight TDs can be directly applied to the human body to harvest electrical energy from physiological thermoregulation. Heat flow from the human body varies according to body location, estimated from 1 to 20 mW/cm^2 at 22 °C average ambient temperature.[5,43] Capturing even a fraction of one percent of this available heat would yield μW per cm^2, which suggests that low-power medical devices and sensors could be powered by wearable CNT-TDs. More generally, as the power-per-function of personal devices and IoT nodes continues to decrease, the potential for TDs such as these will continue to increase, either as outright replacements for, or as integral charging supplements to, conventional batteries.

See the supplementary material for additional information on the sample images and TEM heating chips.

The authors would like to thank Dr. Randall M. Stoltenberg for valuable discussions about aerosol jet printing. We thank Ms. Injung Lee for the schematic drawing of aerosol jet printing and Mr. Kei Takano for the discussions about e-DIPS CNTs. We also thank Dr. Mary Tang, Dr. Michelle Rincon, and Dr. Swaroop Kommera for their Stanford Exfab support. Part of this work was performed at the Stanford Nano Shared Facilities (SNSF) and Stanford Nanofabrication Facility (SNF), supported by the National Science Foundation under Award No. ECCS-1542152. The authors are most grateful to Daihen Corporation and the Stanford SystemX Alliance for their generous support for this research.

DATA AVAILABILITY

The data that support the findings of this study are available from the corresponding author upon reasonable request.

REFERENCES

[1]*Energy Flow Charts: Charting the Complex Relationships among Energy, Water, and Carbon* (Lawrence Livermore National Laboratory and the Department of Energy, 2020).
[2]J. L. Blackburn, A. J. Ferguson, C. Cho, and J. C. Grunlan, Adv. Mater. **30**, 1704386 (2018).
[3]C. Ou, A. L. Sangle, A. Datta, Q. Jing, T. Busolo, T. Chalklen, V. Narayan, and S. Kar-Narayan, ACS Appl. Mater. Interfaces **10**, 19580 (2018).
[4]X. Crispin, Nat. Energy **1**, 16037 (2016).
[5]J.-H. Bahk, H. Fang, K. Yazawa, and A. Shakouri, J. Mater. Chem. C **3**, 10362 (2015).
[6]S. K. Yee, N. E. Coates, A. Majumdar, J. J. Urban, and R. A. Segalman, Phys. Chem. Chem. Phys. **15**, 4024 (2013).
[7]K. C. See, J. P. Feser, C. E. Chen, A. Majumdar, J. J. Urban, and R. A. Segalman, Nano Lett. **10**, 4664 (2010).
[8]Y. Du, K. F. Cai, S. Chen, P. Cizek, and T. Lin, ACS Appl. Mater. Interfaces **6**, 5735 (2014).
[9]M. Culebras, C. M. Gómez, and A. Cantarero, J. Mater. Chem. A **2**, 10109 (2014).
[10]O. Bubnova, Z. U. Khan, A. Malti, S. Braun, M. Fahlman, M. Berggren, and X. Crispin, Nat. Mater. **10**, 429 (2011).
[11]G.-H. Kim, L. Shao, K. Zhang, and K. P. Pipe, Nat. Mater. **12**, 719 (2013).
[12]S. Iijima and T. Ichihashi, Nature **363**, 603 (1993).
[13]D. S. Bethune, C. H. Klang, M. S. de Vries, G. Gorman, R. Savoy, J. Vazquez, and R. Beyers, Nature **363**, 605 (1993).
[14]L. Duclaux, Carbon **40**, 1751 (2002).
[15]Y. Zhao, J. Wei, R. Vajtai, P. M. Ajayan, and E. V. Barrera, Sci. Rep. **1**, 83 (2011).
[16]H. Wang, G. I. Koleilat, P. Liu, G. Jiménez-Osés, Y.-C. Lai, M. Vosgueritchian, Y. Fang, S. Park, K. N. Houk, and Z. Bao, ACS Nano **8**, 2609 (2014).
[17]W. Gomulya, G. D. Costanzo, E. J. F. de Carvalho, S. Z. Bisri, V. Derenskyi, M. Fritsch, N. Fröhlich, S. Allard, P. Gordiichuk, A. Herrmann, S. J. Marrink, M. C. dos Santos, U. Scherf, and M. A. Loi, Adv. Mater. **25**, 2948 (2013).
[18]Y. Miyauchi, M. Iwamura, S. Mouri, T. Kawazoe, M. Ohtsu, and K. Matsuda, Nat. Photonics **7**, 715 (2013).
[19]L. D. Hicks and M. S. Dresselhaus, Phys. Rev. B **47**, 16631 (1993).
[20]A. Shakouri, Annu. Rev. Mater. Res. **41**, 399 (2011).
[21]Y. Nakai, K. Honda, K. Yanagi, H. Kataura, T. Kato, T. Yamamoto, and Y. Maniwa, Appl. Phys. Express **7**, 025103 (2014).
[22]D. Hayashi, T. Ueda, Y. Nakai, H. Kyakuno, Y. Miyata, T. Yamamoto, T. Saito, K. Hata, and Y. Maniwa, Appl. Phys. Express **9**, 025102 (2016).
[23]B. A. MacLeod, N. J. Stanton, I. E. Gould, D. Wesenberg, R. Ihly, Z. R. Owczarczyk, K. E. Hurst, C. S. Fewox, C. N. Folmar, K. Holman Hughes, B. L. Zink, J. L. Blackburn, and A. J. Ferguson, Energy Environ. Sci. **10**, 2168 (2017).
[24]N. Feng, C. Gao, C.-Y. Guo, and G. Chen, ACS Appl. Mater. Interfaces **10**, 5603 (2018).
[25]T. Saito, S. Ohshima, W.-C. Xu, H. Ago, M. Yumura, and S. Iijima, J. Phys. Chem. B **109**, 10647 (2005).
[26]F. M. Winnik, M. A. Winnik, and S. Tazuke, J. Phys. Chem. **91**, 594 (1987).
[27]C. J. Drummond, S. Albers, and D. N. Furlong, Colloids Surf. **62**, 75 (1992).
[28]S. C. Shit and P. M. Shah, J. Polym. **427259**, 1 (2014).
[29]Q. Yang, L. Shuai, J. Zhou, F. Lu, and X. Pan, J. Phys. Chem. B **112**, 12934 (2008).
[30]J.-P. Piret, S. Detriche, R. Vigneron, S. Vankoningsloo, S. Rolin, J. H. Mejia Mendoza, B. Masereel, S. Lucas, J. Delhalle, F. Luizi, C. Saout, and O. Toussaint, J. Nanopart. Res. **12**, 75 (2010).
[31]T. Seifert, M. Baum, F. Roscher, M. Wiemer, and T. Gessner, Mater. Today Proc. **2**, 4262 (2015).
[32]A. A. Gupta, A. Bolduc, S. G. Cloutier, and R. Izquierdo, IEEE International Symposium on Circuits and Systems (2016), p. 866.
[33]B. Clifford, D. Beynon, C. Phillips, and D. Deganello, Sens. Actuators, B **255**, 1031 (2018).
[34]X.-G. Li, M.-R. Huang, and H. Bai, J. Appl. Polym. Sci. **73**, 2927 (1999).
[35]O. W. Guirguis and M. T. H. Moselhey, Nat. Sci. **4**, 57 (2012).
[36]D. Hayashi, Y. Nakai, H. Kyakuno, T. Yamamoto, Y. Miyata, K. Yanagi, and Y. Maniwa, Appl. Phys. Express **9**, 125103 (2016).
[37]Y. Nonoguchi, M. Nakano, T. Murayama, H. Hagino, S. Hama, K. Miyazaki, R. Matsubara, M. Nakamura, and T. Kawai, Adv. Funct. Mater. **26**, 3021 (2016).
[38]W. Huang, E. Tokunaga, Y. Nakashima, and T. Fujigaya, Sci. Technol. Adv. Mater. **20**, 97 (2019).
[39]Y. Nonoguchi, A. Takata, C. Goto, T. Kitano, and T. Kawai, Sci. Technol. Adv. Mater. **19**, 581 (2018).
[40]D. Estrada and E. Pop, Appl. Phys. Lett. **98**, 073102 (2011).
[41]J. Yang, M. Shen, Y. Yang, W. J. Evans, Z. Wei, W. Chen, A. A. Zinn, Y. Chen, R. Prasher, T. T. Xu, P. Keblinski, and D. Li, Phys. Rev. Lett. **112**, 205901 (2014).
[42]F. Lian, J. P. Llinas, Z. Li, D. Estrada, and E. Pop, Appl. Phys. Lett. **108**, 103101 (2016).
[43]V. Leonov, ISRN Renewable Energy **785380**, 1 (2011).